Journal of Power Sources 195 (2010) 7983–7990

Contents lists available at ScienceDirect

Journal of Power Sources

journal homepage: www.elsevier.com/locate/jpowsour

Sea urchin-like mesoporous carbon material grown with carbon nanotubes as a cathode catalyst support for fuel cells

Ping-Lin Kuo*, Chun-Han Hsu, Wan-Ting Li, Jing-Yi Jhan, Wei-Fu Chen

Department of Chemical Engineering, National Cheng Kung University, Tainan 70101, Taiwan, ROC

ARTICLE INFO

Article history:
Received 28 April 2010
Received in revised form 14 June 2010
Accepted 15 June 2010
Available online 23 June 2010

Keywords:
Carbon support
Fuel cells
Catalyst
Cathode
Stabilizer

ABSTRACT

A sea urchin-like carbon (UC) material with high surface area (416 $m^2 g^{-1}$), adequate electrical conductivity (59.6 $S cm^{-1}$) and good chemical stability was prepared by growing carbon nanotubes onto mesoporous carbon hollow spheres. A uniform dispersion of Pt nanoparticles was then anchored on the UC, where the Pt nanoparticles were prepared using benzylamine as the stabilizer. For this Pt loaded carbon, cyclic voltammogram measurements showed an exceptionally high electrochemically active surface area (EAS) (114.8 $m^2 g^{-1}$) compared to the commonly used commercial E-TEK catalyst (65.2 $m^2 g^{-1}$). The durability test demonstrates that the carbon used as a support exhibited minor loss in EAS of Pt. Compared to the E-TEK (20 wt%) cathode catalyst, this Pt loaded UC catalyst has greatly enhanced catalytic activity toward the oxygen reduction reaction, less cathode flooding and considerably improved performance, resulting in an enhancement of ca. 37% in power density compared with that of E-TEK. Based on the results obtained, the UC is an excellent support for Pt nanoparticles used as cathode catalysts in proton exchange membrane fuel cells.

1. Introduction

Proton exchange membrane fuel cells (PEMFCs) have been of great interest as future energy sources for various applications, and have attracted much research work in this field [1–3]. However, the commercial viability of the technology of PEMFCs has been hindered by several challenges, including poor kinetics of the oxygen reduction reaction (ORR), the high cost of noble metal catalysts and the loss of electrochemically active surface areas (EAS) of Pt [4–6]. In fuel cell electrodes, the catalytic activity of a fuel cell catalyst based on Pt is related to the dispersion and the size distribution of the catalyst and closely linked to the characteristics of the carbon support [7–10]. An increase in the dispersion of the catalyst should lead to an enhancement of the kinetics, particularly of the ORR, whose rate is an important limiting factor in fuel cell performance. Catalyst support technology has been proven as an effective approach to lowering the usage of noble metal while simultaneously improving the catalytic activity of the supported catalysts. The key properties of carbon supports are a relatively large surface area, good electrical conductivity, and an accessible porosity. Rather than the most frequently employed supports at present, such as carbon black and activated carbon, carbon nanotubes (CNTs), carbon nanofibers, or hollow nanospheres have proven to better supports for electrocatalysts [11–15]. CNTs have excellent electrical conductivity but, they exhibit a poor pore development and low surface area. Pores and surface area ensure simultaneous contact between the reactant fuel and the catalyst, which allows the electrochemical reactions to take place. In contrast, mesoporous carbon has high mesoporosity and relatively low microporosity, but has an amorphous framework and poor electrical conductivity [16–19]. Therefore, it would be of great interest to develop a novel material to combine the advantages of these two materials together.

The present work aims at obtaining a deeper insight into the preparation of sea urchin-like carbon (UC) by growing CNTs on mesoporous carbon hollow spheres (MCHS). This new material offers the advantageous features of large surface area, high electronic conductivity, good chemical stability and hydrophobicity. This UC was used as a catalyst support for application in fuel cell electrodes. A uniform dispersion of Pt nanoparticles was then anchored on the UC, where the Pt nanoparticles were prepared using benzylamine as the stabilizer. The EAS and durability test of the Pt loaded UC (Pt/UC) were measured by cyclic voltammetry

* Corresponding author. Tel.: +886 6 275 7575; fax: +886 6 276 2331.
E-mail address: plkuo@mail.ncku.edu.tw (P.-L. Kuo).

0378-7753/$ – see front matter © 2010 Elsevier B.V. All rights reserved.
doi:10.1016/j.jpowsour.2010.06.048

(CV) and showed excellent performance. Finally, preliminary tests of membrane electrode assemblies (MEA), using Pt/UC as catalyst at the cathode, were carried out in a single 5 cm^2 PEMFC.

2. Experimental

2.1. Synthesis of UC

The MCHS were synthesized using a method reported in literature [20,21]. The MCHS were dispersed in iron ionic $Fe(NO_3)_3$ solution with an $[Fe^{3+}]$ concentration of 5×10^{-3} M. The solution was stirred overnight, and the sample was later filtered and dried under vacuum at 70 °C. Then the powder was placed in a quartz tube where Argon gas was used as the carrier gas at a flow rate of 100 standard cubic centimeters per minute (sccm) during the entire process. Hydrogen gas (99.9%) was subsequently used to reduce the iron at a steady flow rate of 20 sccm at 500 °C. Then, CNTs were grown from iron catalysts on carbon spheres through reaction with acetylene at a steady flow rate of 20 sccm at 700 °C with different time conditions. Finally, $HCl_{(conc.)}$ was used to remove the iron catalysts on the UC. MCHS with various lengths of CNTs are denoted as UC_χ, with χ representing the growth time (i.e. 20 and 45 min) of CNTs.

2.2. Synthesis of carbon-supported Pt catalysts

The carbon material supported Pt catalysts were prepared by the reduction of $PtCl_6^{2-}$ using tri-sodium citrate, while the stabilization and deposition of Pt particles on the carbon supports were accomplished by the amino-containing stabilizer [22,23]. First, H_2PtCl_6 aqueous solution was mixed with excess solids of tri-sodium citrate in boiling water. When the color of the solution changed from yellowish to brown, heating was stopped immediately. After cooling down, benzylamine was dissolved in the above solution with carbon material. In this experiment, the catalyst ratio of 20 wt% was synthesized and real loadings of Pt were measured by thermogravimetric analysis (TGA). Residue solids were washed by copious amounts of deionized water to remove $[Cl^-]$. In order to remove the stabilizer on the electrocatalysts, heat treatment was performed at 400 °C for 4 h under a H_2 atmosphere.

2.3. Methods of characterization

X-ray photoelectron spectroscopy (XPS) measurements were carried out with a VG Scientific ESCALAB 210 electron spectrometer using Mg-K_α radiation under a vacuum of 2×10^{-8} Pa. The morphological characterization was performed by scanning electron microscope (SEM) using a JEOL JEM6700 FESEM operating at 10 kV. Transmission electron microscopy (TEM) was conducted using a Hitachi H-7500 microscope operating at 80 kV. TG analysis was performed on a thermogravimetric analyzer (TGA Q-50) over a temperature range of 50–800 °C at a heating rate of 20 °C min^{-1}. X-ray powder diffraction (XRD) was performed on a Rigaku RINT2100 X-ray diffractometer with Cu-K_α radiation operated at 30 kV and 30 mA. Specific surface areas of the prepared carbons were determined using the Brunauer–Emmett–Teller (BET) method on a Micromeritics ASAP 2020 instrument. A CHI-608A potentiostat/galvanostat and a conventional three-electrode test cell were used for electrochemical measurements. An Ag/AgCl/KCl (3 M) electrode was used as a reference. All potential in this study, however, are given relative to the reversible hydrogen electrode (RHE). Glassy carbon disk electrode (5 mm diameter, Pine) served as the substrate for the supported catalyst. An aliquot of catalyst suspension was transferred onto the carbon substrate, leading to a catalyst loading of 50.5 μg catalyst cm^{-2} for Pt/MCHS, Pt/UC_{20}, Pt/UC_{45} and E-TEK. The CV test for accelerated durability was performed on the working electrode by cycling the voltage between 0 and 1.23 V versus RHE in 0.1 M $HClO_4$ solution. The scan rate was 20 mV s^{-1}. The electrochemical surface areas were calculated from the H_2 adsorption–desorption peaks of the CV cycle. In total, 5000 CV cycles were performed for each case.

Single fuel cell test was evaluated using a unit cell with an active area of 5 cm^2 fed with hydrogen and oxygen at the anode and cathode for a rate of 200 ml min^{-1}. The MEA for the single cell test was fabricated as follows. Catalyst ink was prepared by mixing Pt/C catalyst powder with water (2.0 ml for 1.0 g of electrocatalyst), and then adding iso-propanol (20 ml for 1.0 g of electrocatalyst) to avoid any ignition. 5% Nafion dispersion (Dupont) was added (0.8 g solid Nafion for 1.0 g of catalyst) to the catalyst slurry. Catalyst coating on gas diffusion layer (GDL, 50 wt% wet-proofing carbon paper, Toray) with 5 cm^2 active area was fabricated by brushing Pt/C catalyst ink. The catalyst loadings on the anode and cathode layers were both 0.5 mg Pt cm^{-2}. The catalyst-coated GDLs were hot-pressed with Nafion-117 membrane (Du Pont) at 140 °C under 30 kg cm^{-2} of pressure.

3. Results and discussion

3.1. Synthesis and characterization of UC material

UC was prepared by growing curled CNTs on MCHS to incorporate the unique structures and properties of two types of nanostructured carbon materials. The MCHS were synthesized by templating method, starting with phenol formaldehyde polymer as the carbon precursor and using gelatin as a structure-directing agent [20,21]. Fig. 1a shows that the carbon spheres were uniform and spherical with a diameter of approximately 1.0 μm. Examination of the broken spheres confirmed that they have spherical hollow cores with a shell thickness of about 100 nm. The MCHS were used as a substrate for growing CNTs to form UC materials. Fig. 1b and c shows the SEM images of UC_{20} and UC_{45}, and illustrates that the curled CNTs were clearly produced on the surface of carbon spheres. As the growth time of CNTs was increased from 20 to 45 min, the length of the CNTs increased.

Table 1
Surface structure parameters and electron conductivity for MCHS, UC_{20}, UC_{45}, and commercial XC-72 carbon supports.

Sample	S_{BET}[a] (m^2 g^{-1})	S_{micro}[b] (m^2 g^{-1})	$S_{meso\text{-}macro}$[c] (m^2 g^{-1})	V_{total}[d] (m^3 g^{-1})	Conductivity[e] (S cm^{-1})
MCHS	717	191	526	1.20	7.4
UC_{20}	416	22	394	1.02	47.3
UC_{45}	357	12	345	1.04	59.6
XC-72	217	68	149	0.57	29.2

[a] S_{BET}, BET surface area.
[b] S_{micro}, micropore surface area.
[c] $S_{meso\text{-}macro}$, mesopore and micropore surface area.
[d] V_{total}, total pore volume.
[e] Conductivity, the electron conductivities were measured by adding 5% PTFE in the sample.

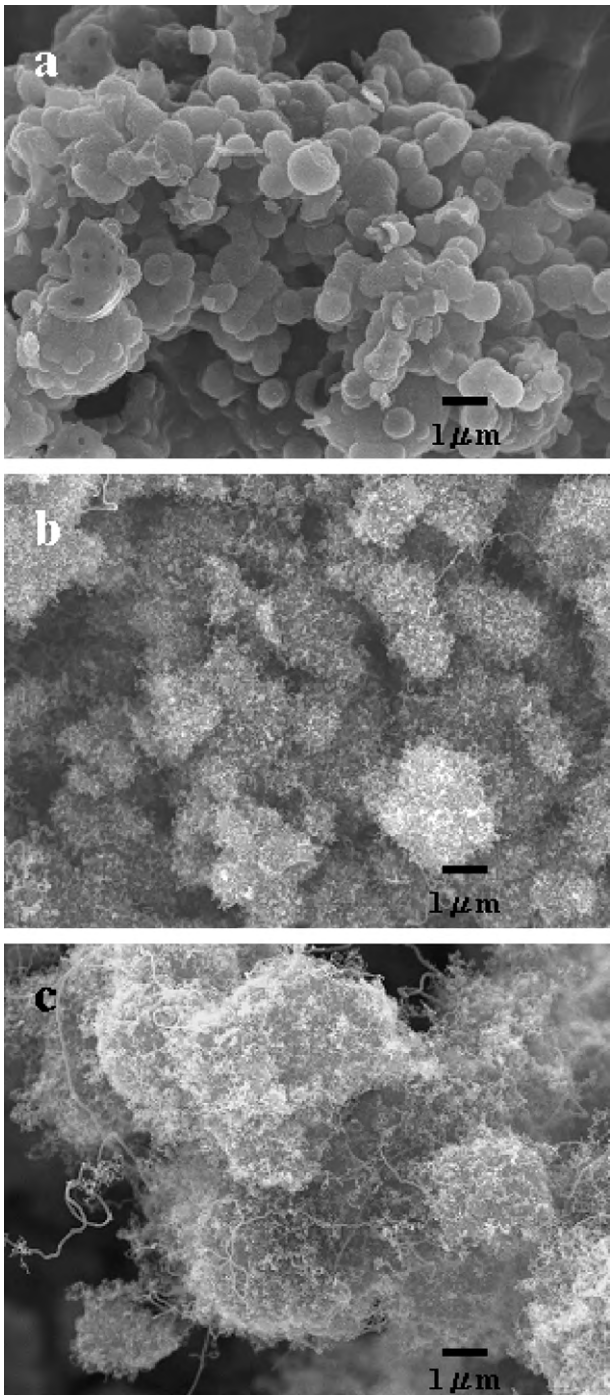

Fig. 1. Typical FESEM images of the (a) MCHS, (b) UC_{20}, (C) UC_{45}.

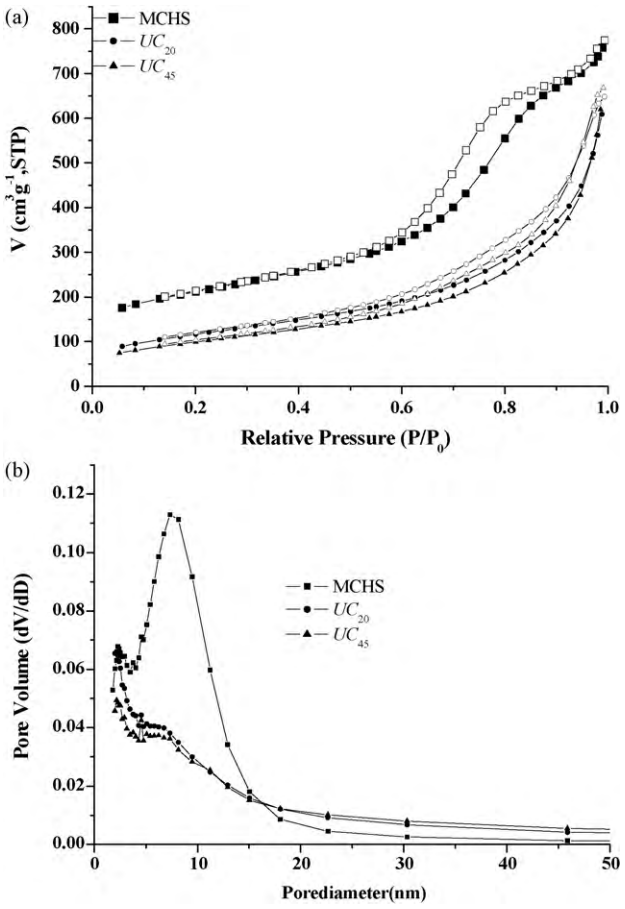

Fig. 2. (a) Nitrogen adsorption and desorption isotherms and (b) pore size distribution of MCHS, UC_{20} and UC_{45}.

The nitrogen adsorption–desorption isotherms and pore size distributions were used to characterize the pore structures of the MCHS with different lengths of CNTs, as shown in Fig. 2. Structural parameters for the MCHS, UC, and Vulcan XC-72 derived from the nitrogen adsorption–desorption isotherms are summarized in Table 1. The nitrogen adsorption–desorption curves confirm that the prepared MCHS (Fig. 2a) can be classified as the type IV typical mesoporous material. Fig. 2b reveals that the MCHS have a narrow pore size distribution centered at 7.5 nm and a high BET surface area (S_{BET}) of 717 $m^2\,g^{-1}$, with a total pore volume (V_{pore}) of 1.20 $cm^3\,g^{-1}$, as shown in Table 1. After growth of CNTs on the MCHS for 20 and 45 min, the BET surface area decreased to 416 and 357 $m^2\,g^{-1}$, respectively. As shown in Table 1, the total pore volume decreased from 1.2 to 1.04 $cm^3\,g^{-1}$ as the growth time increase from 0 to 45 min. As a comparison, the commercially produced Vulcan XC-72 carbon exhibited a low surface area of 217 $m^2\,g^{-1}$ and pore volume of 0.57 $cm^3\,g^{-1}$. It is known that, for carbon-supported Pt catalysts, Pt particles have to be well dispersed on conductive carbon supports and in small sizes to effectively utilize these metals. Higher surface areas of carbon supports increase depositing sites for the small Pt particles. However, the microporosity of the carbon support would reduce the accessibility of deposited Pt owing to the hindering of the contact between the Pt surface and the fuel (e.g. hydrogen or methanol). Therefore, the microporosity of these carbon materials was calculated based on the surface area that limits the pore diameter to less than 2.0 nm. As seen in Table 1, the prepared UCs have a relatively lower micropore surface area of 22 and 12 $m^2\,g^{-1}$ for UC_{20} and UC_{45}, respectively, as compared with that of the Vulcan XC-72 carbon (68 $m^2\,g^{-1}$).

The electrical conductivity of the UC was further characterized, also shown in Table 1. The MCHS exhibited an electrical conductivity of 7.4 S cm^{-1}, while UC_{20} and UC_{45} showed much higher electron conductivities, i.e. 47.3 and 59.6 S cm^{-1}, respectively. Evidently, the growth of CNTs onto MCHS effected a remarkable increase in electrical conductivity, which is significantly better than XC-72 (29.2 S cm^{-1}). This reveals that the CNTs on MCHS enable the conduction of electrons among carbon spheres more effectively than XC-72.

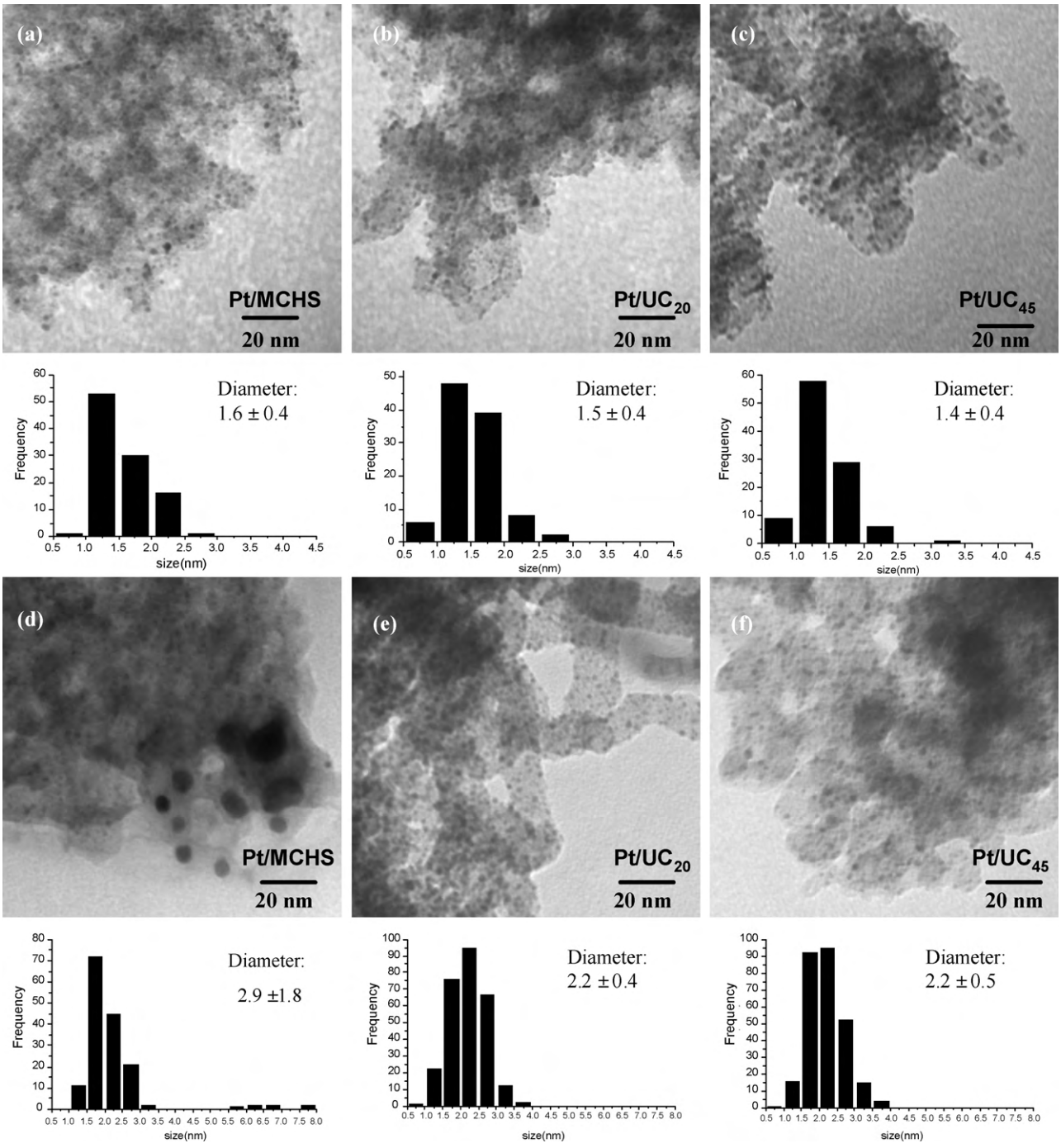

Fig. 3. TEM images of as-prepared (a) Pt/MCHS, (b) Pt/UC_{20}, and (c) Pt/UC_{45} and heat-treated (d) Pt/MCHS, (e) Pt/UC_{20}, and (f) Pt/UC_{45} catalysts.

3.2. Deposition of Pt nanoparticles on UC

The UC material is expected to be utilized as a Pt support for application in electrocatalysts. In this work, carbon-supported Pt nanoparticles were prepared by a benzylamine-assisting method superior to our current stabilizer [22–24]. We use benzylamine molecules as a stabilizer to protect Pt nanoparticles so that damage to the graphene structures of carbon materials is prevented. The TEM images of the benzylamine-stabilized Pt nanoparticles supported on MCHS, UC_{20}, and UC_{45} are shown in Fig. 3a–c, respectively. Pt nanoparticles, which were well dispersed on the carbon surface, with a diameter of about 1.5 nm were obtained. This result indicates that benzylamine provides very good stabilization for Pt. Stabilization of the Pt particles by benzylamine can be discussed mainly from the viewpoint of complexing ability and π–π interaction: the amine group is a highly effective chelating agent for metal atoms, and meanwhile, the benzyl rings surrounding the complexed metal core simultaneously separate the particles from each other and promote the Pt nanoparticles to adsorb onto the surface of carbon supports through the π–π interaction. The morphology of the carbon-supported Pt nanoparticles after thermal treatment was investigated by TEM to determine the quality of the dispersion. Fig. 3d–f displays the TEM images of the samples after thermal treatment in a H_2 flow at 400 °C for 4 h. The average diameters of the samples before and after calcinations are displayed in Table 2. It can be seen that the particle sizes increased slightly to

Table 2
Mean diameters and electrochemical active surface area of as-prepared and heat-treated Pt/C catalysts with different carbon supports.

Sample	Pt content (wt%)	d (nm)		EAS ($m^2\ g^{-1}$ Pt)		
		Before calcination	After calcination	Before calcination	After calcination	After 5000 cycles
Pt/MCHS	19.7	1.6 ± 0.4	2.9 ± 1.8	51.7	61.4	47.0
Pt/UC_{20}	17.2	1.5 ± 0.4	2.2 ± 0.4	52.7	78.8	73.3
Pt/UC_{45}	18.6	1.4 ± 0.4	2.2 ± 0.5	64.4	114.8	94.1
E-TEK	20.0	–	2.4 ± 0.5	–	65.2	49.2

2.9, 2.2 and 2.2 nm for Pt/MCHS, Pt/UC_{20} and Pt/UC_{45}, respectively, after calcinations. No serious agglomeration or fusion occurred, and the quality of dispersion for Pt remained high. As shown in Table 2, the particle sizes of Pt on UC_{20} and UC_{45} after calcinations were smaller than the size of commercial E-TEK 20 wt% Pt/C (2.4 nm).

The powder XRD patterns of Pt supported on the heat-treated MCHS, UC_{20} and UC_{45} are shown in Fig. 4. The diffraction peaks in the XRD pattern at 2θ of 39.6°, 46.1°, 67.5°, and 81.2° can be assigned to be the reflections of the (1 1 1), (2 0 0), (2 2 0), and (3 1 1) planes of the face-centered-cubic (fcc) Pt, respectively. The bandwidth became slightly sharper for the MCHS-supported Pt catalyst, indicating an increase in particle size. Grain sizes of 2.2 nm were calculated for Pt nanoparticles supported on the UC from measurement of the broadening of the (2 2 0) peaks using the Scherrer equation, which is smaller than that of the Pt supported on MCHS (3.0 nm). The calculated grain sizes of the UC supported Pt nanoparticles are in agreement with those determined by TEM. This demonstrates that the agglomeration which occurred among the supported Pt nanoparticles was not serious.

For a benzylamine-stabilized Pt/C catalyst, the interaction between benzylamine and Pt was characterized by the N 1s line of the X-ray photoemission spectroscopy (XPS), as shown in Fig. 5a. The N 1s line was deconvoluted into three superimposed peaks at 397.6, 399.3 and 401.9 eV. The peaks at 399.3 and 401.9 eV are characteristic peaks for free amine and protonated ammonium ions, respectively. The peak component at 397.6 eV demonstrates the presence of a nitride bonding (Pt–N) between the head-on N atoms of benzylamine and the surface Pt atoms of Pt nanoparticles. This result evidently proves the bi-functional stabilizing mechanism of benzylamine to Pt particles. In Fig. 5b, the Pt 4f line showed two pairs of peaks from the spin–orbital splitting of the $4f_{7/2}$ and $4f_{5/2}$. The most intense doublets observed at 71.3 and 74.5 eV are attributed to zero-valent Pt (Pt(0)). This demonstrates that the well dispersed and Pt(0)-dominated catalysts have been successfully prepared by this method.

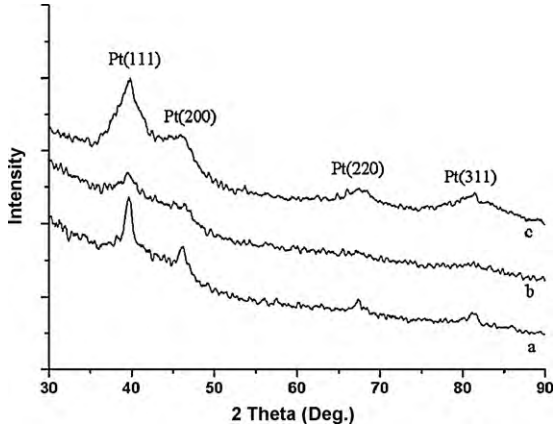

Fig. 4. Typical X-ray diffraction patterns for the (a) Pt/MCHS, (b) Pt/UC_{20}, and (c) Pt/UC_{45} catalysts.

3.3. Electrochemical properties of the UC supported Pt catalyst

3.3.1. Electrochemical active surface area

To illustrate how the stabilizer layer of benzylamine affects electrochemical properties of Pt, the CVs of UC supported Pt catalysts before and after calcination (Fig. 6a and b) were measured and compared to those of MCHS-supported Pt and E-TEK Pt/C catalysts. The EAS were estimated by the integrated charge (after excluding the double layer charging effect) in the hydrogen adsorption–desorption region [25]. Before calcination (Fig. 6a), the hydrogen adsorption–desorption characteristic peaks in the potential range from 0 to 0.3 V using RHE as reference are small. After calcination (Fig. 6b), the hydrogen adsorption–desorption peaks become strong and well-featured. This indicates that the decomposition of benzylamine has brought about the exposure of the Pt active site to the electrolyte solution.

As shown in Table 2, the EAS in the presence of benzylamine are 51.7, 52.7 and 64.4 $m^2\ g^{-1}$ for Pt/MCHS, Pt/UC_{20} and Pt/UC_{45}, respectively. After calcination, the EAS became 61.4, 78.8 and

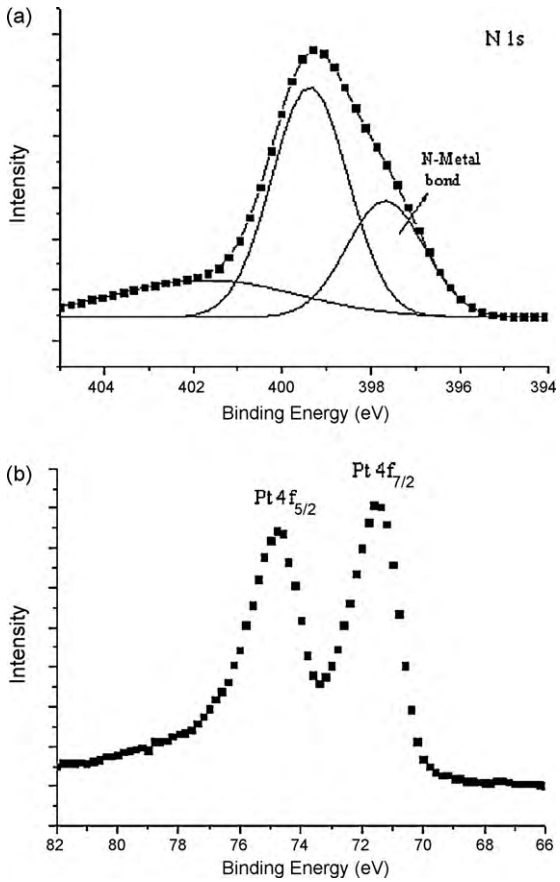

Fig. 5. XPS spectra of (a) N 1s lines for as-prepared Pt/C catalyst and (b) Pt 4f region for Pt/C catalyst after thermal treatment.

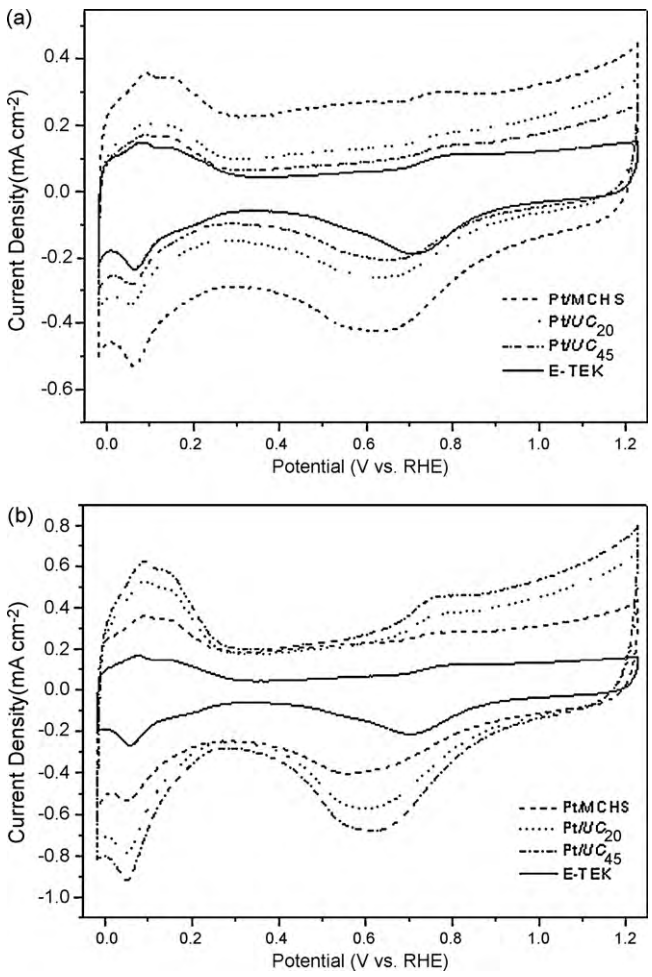

Fig. 6. Cyclic voltammograms of various carbon supports supported Pt catalysts (a) before and (b) after calcination. CVs were obtained at a scan rate of 20 mV s^{-1} in 0.1 M $HClO_4$.

114.8 m^2 g^{-1}, respectively. Again, decomposition of benzylamine enables Pt to be more exposed to hydrogen and to show more activity. It can be seen that the thermal treatment made Pt/MCHS, Pt/UC_{20} and Pt/UC_{45} to increase 19%, 50% and 78% increase in the EAS, respectively. As mentioned-above, the EAS values of Pt/UC_{20} and Pt/UC_{45} are higher than that of Pt/MCHS, which indicates that the Pt nanoparticles deposited on UC exposed more active sites than those in the pores of the MCHS after calcination. The different degree in enhanced EAS area depends on where the Pt nanoparticles are deposited. As mentioned in the previous section, the average pore size of MCHS was 7.5 nm, calculated by the BJH methode, thus, the benzylamine-stabilized 1.5 nm Pt nanoparticles can fall through the pores of the MCHS. Since benzylamine is in excess relative to Pt molarity, extra benzylamine can be adsorbed by the mesopores of the MCHS. During calcination, both the coordinated and extra benzylamines were burned and became residual char. On the surface of the Pt nanoparticles, the existence of carbonaceous char can separate particles from each other, thus the well dispersed 2.9 nm Pt nanocatalysts were obtained. However, the char may lay over the Pt active sites and obstruct the contact of electrolyte solutions or fuels with Pt sites. Thus, we observed a smaller degree in enhanced EAS for the MCHS-supported Pt catalyst. For UC, the nanotubes do not have the pores that cause the hindrance to the active sites on the Pt particles. Therefore, we observed a higher degree in enhanced EAS after burning the benzylamines for the UC supported Pt catalysts. It can be concluded from these results that Pt nanoparticles supported on UC have a better utilization of Pt active sites than on MCHS. Moreover, the EAS values of Pt/UC_{20} and Pt/UC_{45} are all significantly higher than the 65.2 m^2 g^{-1} of 20% E-TEK Pt/C. It is known that the higher EAS the catalyst has, the better the activity for ORR the catalyst possesses.

3.3.2. Durability test of Pt catalyst and carbon support

To be a candidate for cathode material of PEMFC, oxidation stability of carbon supports and the corresponding durability of catalyst particles are major requirements for cathode catalysts. CV measured under hydrogen adsorption–desorption can be used to not only determine the Pt active surface area as above-mentioned, but also to evaluate the stability of the catalyst. The degradation of an electrocatalyst can be characterized by measuring the repeated CV cycles with the appropriate lower and upper potential limits in an acid solution [26–28]. Hereafter, the measurement of CV curves for Pt/MCHS, Pt/UC_{20}, Pt/UC_{45} and E-TEK Pt/C was conducted by cycling the electrode potential between 0 and 1.23 V using RHE as reference at a scan rate of 20 mV s^{-1} in a 0.1 M $HClO_4$ solution. As shown in Fig. 7b and c, The Pt EAS of the Pt/UC_{20} and Pt/UC_{45} only decrease about 7% and 18% (Table 2) after 5000 cycles, respectively. However, the Pt EAS of E-TEK Pt/C (Fig. 7d) and Pt/MCHS significantly decrease by about 25% and 23% after 5000 cycles, respectively, indicating that the growth of CNTs onto MCHS can provide much higher durability. The MCHS has been characterized as amorphous phase-rich carbon and is easily oxidized. Thus, the oxidation during potential cycling may induce a surface structural change of the nanopores so as to cause the decrease of surface area [28]. On a support with a smaller surface area, the aggregation of Pt particles occurs more easily, and results in the decreased EAS.

3.4. Performance of the cathode of PEMFC

The polarization behavior and power density curve of the single PEMFC at 70 °C using Pt/UC_{45} as the cathode was compared to that using E-TEK Pt/C and Pt/MCHS as the cathode material (Fig. 8), where E-TEK 20% Pt/XC-72 was used as anode for each fuel cell test. Pt loading was 0.5 mg cm^{-2} both at cathode and anode. At 0.8 V, the activation polarization is mainly affected by the activity of the catalyst. Thus, all of the measurements were carried out at 0.8 V. The Pt/UC_{45} catalyst showed a current density of 120 mA cm^{-2}, which is remarkably higher than the E-TEK catalyst (105 mA cm^{-2}) and is more than three times as high as the Pt/MCHS catalyst (40 mA cm^{-2}). The UC supported catalyst exhibited both higher initial and final current density of oxygen reduction than the E-TEK catalyst and Pt/MCHS. Moreover, Pt/UC_{45} exhibited a higher maximum power density (323 mW cm^{-2}) than those of the E-TEK catalyst (235 mW cm^{-2}) and the Pt/MCHS catalyst (257 mW cm^{-2}). This corresponds to the 37% and 26% increase in oxygen reduction activity for the Pt/UC_{45} catalyst compared to those of the E-TEK catalyst and Pt/MCHS catalysts, respectively. Such a large improvement may be related to the unique structural properties of the UC. This is derived from: (1) the higher surface areas and larger pore volumes of the UC, which allow for a greater degree of catalyst dispersion; and (2) the better electrical conductivity compared to MCHS and XC-72. Furthermore, at a current density higher than 350 mA cm^{-2}, the curves of potential and power density for E-TEK drop abruptly; however, those for Pt/UC_{45} and Pt/MCHS, all decreased gradually and higher than those for E-TEK. For the Pt/UC_{45} based cathode, the growth of CNTs on the MCHS may lead to the higher hydrophobicity and therefore the less cathode flooding.

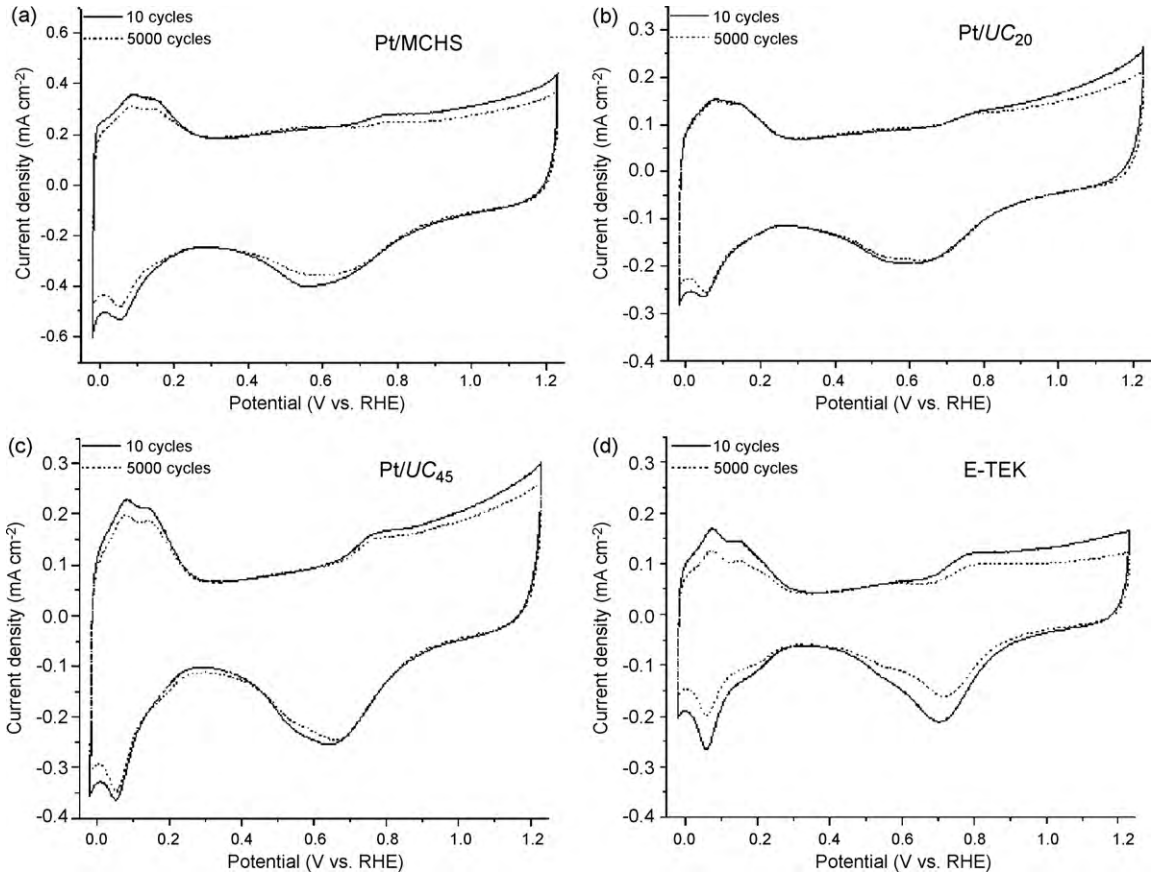

Fig. 7. Cyclic voltammograms of various carbon supports supported Pt catalyst at different scan cycles in 0.1 M $HClO_4$. Scan rate: 20 mV s^{-1}.

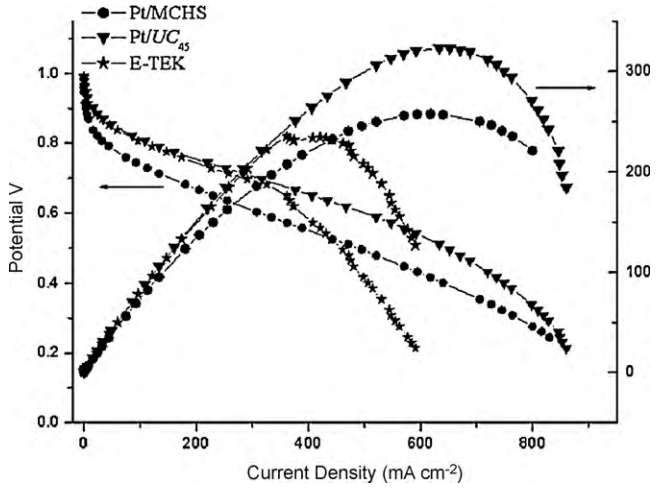

Fig. 8. (a) Polarization curves and (b) power density plots of PEMFC using Pt catalyst supported on MCHS, UC_{45} and commercial E-TEK catalyst at 70 °C.

4. Conclusions

The growth of CNT on the MCHS was realized by CVD using Fe as catalyst. Pt deposition on the UC was then conducted by benzylamine as a stabilizer to Pt nanoparticles. CV measurements show an exceptionally high EAS (114.8 m^2 g^{-1}) compared to the commonly used commercial E-TEK catalyst (65.2 m^2 g^{-1}). Furthermore, the durability test demonstrated that UC as a support exhibited less Pt surface area loss without sacrificing catalytic activity. This is considered to be due to the unique structural properties of the UC including large surface area, high electron conductivity, and well developed interconnected porosity, which can support Pt nanoparticles to be in uniform dispersion and of small particle size. Compared to the Pt/XC-72 cathode catalyst, the Pt/UC catalyst has demonstrated greatly enhanced catalytic activity toward ORR, less cathode flooding and considerably improved PEMFC performance. Based on the results obtained, the UC is an excellent support for Pt nanoparticles for cathode catalysts in PEMFC.

References

[1] S. Litster, G. McLean, J. Power Sources 130 (1–2) (2004) 61–76.
[2] H. Liu, C. Song, L. Zhang, J. Zhang, H. Wang, D.P. Wilkinson, J. Power Sources 155 (2) (2006) 95–110.
[3] Y.G. Guo, J.S. Hu, L.J. Wan, Adv. Mater. 20 (15) (2008) 2878–2887.
[4] X. Wang, W. Li, Z. Chen, M. Waje, Y. Yan, J. Power Sources 158 (1) (2006) 154–159.
[5] K. Wikander, H. Ekstrom, A.E.C. Palmqvist, G. Lindbergh, Electrochim. Acta 52 (24) (2007) 6848–6855.
[6] F. Wen, U. Simon, Chem. Mater. 19 (14) (2007) 3370–3372.
[7] Z. Wen, J. Liu, J. Li, Adv. Mater. 20 (4) (2008) 743–747.
[8] W. Xu, X. Zhou, C. Liu, W. Xing, T. Lu, Electrochem. Commun. 9 (5) (2007) 1002–1006.
[9] H. Du, L. Gan, B. Li, P. Wu, Y. Qiu, F. Kang, et al., J. Phys. Chem. C 111 (5) (2007) 2040–2043.
[10] E. Yoo, T. Okada, T. Kizuka, J. Nakamura, J. Power Sources 180 (1) (2008) 221–226.
[11] A.L. Dick, J. Power Sources 156 (1) (2006) 128–141.
[12] M. Michel, A. Taylor, R. Sekol, P. Podsiadlo, P. Ho, N. Kotov, et al., Adv. Mater. 19 (22) (2007) 3859–3864.
[13] X. Li, I.M. Hsing, Electrochim. Acta 51 (25) (2006) 5250–5258.
[14] G.G. Wildgoose, C.E. Banks, R.G. Compton, Small 2 (2) (2006) 182–193.
[15] K. Lee, J. Zhang, H. Wand, D.P. Wilkinson, J. Appl. Electrochem. 36 (5) (2006) 507–522.
[16] S.H. Joo, S.J. Chol, I. Oh, J. Kwak, Z. Liu, O. Terasaki, et al., Nature 412 (6843) (2001) 169–172.

[17] M. Sevilla, A.B. Fuertes, Carbon 44 (3) (2006) 468–474.
[18] Y. Piao, K. An, T. Yu, T. Hyeon, J. Mater. Chem. 16 (29) (2006) 2984–2989.
[19] H. Chang, S.H. Joo, C. Pak, J. Mater. Chem. 17 (30) (2007) 3078–3088.
[20] Y.C. Lin, C.H. Hsu, H.P. Lin, C.Y. Tang, C.Y. Lin, Chem. Lett. 36 (10) (2007) 1258–1259.
[21] K.W. Chang, Z.Y. Lim, F.Y. Du, Y.L. Yang, C.H. Chang, C.C. Hu, et al., Diam. Relat. Mater. 18 (2–3) (2009) 448–451.
[22] P.L. Kuo, W.F. Chen, H.Y. Huang, I.C. Chang, S.A. Dai, J. Phys. Chem. B 110 (7) (2006) 3071–3077.
[23] W.F. Chen, H.Y. Huang, C.H. Lien, P.L. Kuo, J. Phys. Chem. B 110 (20) (2006) 9822–9830.
[24] C.H. Hsu, H.Y. Liao, P.L. Kuo, J. Phys. Chem. C 114 (17) (2010) 7933–7939.
[25] A. Pozio, M.D.F. Francesco, A. Cemmi, F. Cardellini, L. Giorgi, J. Power Sources 105 (1) (2002) 13–19.
[26] Z. Chen, M. Waje, W. Li, Y. Yan, Angew. Chem. Int. Ed. 46 (22) (2007) 4060–4063.
[27] J. Zhang, K. Sasaki, E. Sutter, R.R. Adzic, Science 315 (5809) (2007) 220–222.
[28] M.K. Debe, A.K. Schmoeckel, G.D. Vernstrorn, R. Atanasoski, J. Power Sources 161 (1) (2006) 1002–1011.